



Nanoscale patterning of graphene through femtosecond laser ablation

R. Sahin, E. Simsek, and S. Akturk

Citation: [Applied Physics Letters](#) **104**, 053118 (2014); doi: 10.1063/1.4864616

View online: <http://dx.doi.org/10.1063/1.4864616>

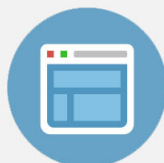
View Table of Contents: <http://scitation.aip.org/content/aip/journal/apl/104/5?ver=pdfcov>

Published by the [AIP Publishing](#)



Re-register for Table of Content Alerts

Create a profile.



Sign up today!



Nanoscale patterning of graphene through femtosecond laser ablation

R. Sahin,¹ E. Simsek,² and S. Akturk^{1,a)}

¹Department of Physics, Istanbul Technical University, Maslak 34469, Istanbul, Turkey

²Electrical and Computer Engineering, The George Washington University, Washington, DC 20052, USA

(Received 15 November 2013; accepted 26 January 2014; published online 7 February 2014)

We report on nanometer-scale patterning of single layer graphene on SiO₂/Si substrate through femtosecond laser ablation. The pulse fluence is adjusted around the single-pulse ablation threshold of graphene. It is shown that, even though both SiO₂ and Si have more absorption in the linear regime compared to graphene, the substrate can be kept intact during the process. This is achieved by scanning the sample under laser illumination at speeds yielding a few numbers of overlapping pulses at a certain point, thereby effectively shielding the substrate. By adjusting laser fluence and translation speed, 400 nm wide ablation channels could be achieved over 100 μm length. Raster scanning of the sample yields well-ordered periodic structures, provided that sufficient gap is left between channels. Nanoscale patterning of graphene without substrate damage is verified with Scanning Electron Microscope and Raman studies. © 2014 AIP Publishing LLC.

[<http://dx.doi.org/10.1063/1.4864616>]

Graphene, a single-layer carbon atoms arranged in a honeycomb structure, has been receiving a growing attention from diverse research fields due to its unique electrical, optical, and mechanical properties.^{1–4} Recent studies show that large area graphene sheets can easily be produced using standard chemical vapor deposition (CVD) method.⁵ High spatial quality, low cost, and straightforward production of single layer graphene (SLG) are advantages of the CVD method. On the other hand, the majority of the graphene applications require its surface to be patterned on micrometer or nanometer scale. Such patternings can be done through lithographical processes.^{6,7} However, fabrication of complex patterns with high resolution and on various substrates still remains challenging. Alternatively, patterning can also be achieved using pulsed-laser ablation. In particular, femtosecond (fs) laser ablation provides high quality and repeatable structures due to its non-thermal nature; hence this method possesses a potential for graphene patterning applications.

In one of the earliest experimental works on the issue, Kalita *et al.* use the fs laser ablation method to produce 5 μm width graphene stripes on glass substrate.⁸ The Raman spectra taken from the ablation region indicates an increase of disorder, yet no formation of amorphous carbon. Zhang *et al.* obtain 25 μm wide channels of graphene-oxide, separated by <2 μm ablation gaps, on glass substrates using direct fs laser cutting.⁹ A detailed study of graphene ablation mechanisms under single-pulse and multi-pulse irradiation conditions is performed by Roberts *et al.*¹⁰ For single-pulse irradiation, a sharp and repeatable ablation threshold and microscopically clean ablation edges are measured. It is also observed that, on multi-shot irradiation, fluences well below the ablation threshold can yield cumulative defect formation and eventual ablation. In the multi-shot irradiation regime, sub-100 nm resolution is demonstrated.¹¹ In this latter work, the focused laser beam profile is also brought to doughnut-shape, thereby yielding sub-diffraction limit nano-ribbons. In an alternative approach, Yoo *et al.* utilize single-pulse fs

laser ablation for generation of graphene folds on SiO₂/Si substrate.¹² The folds exhibit self-formation of graphene ribbons as small as 200 nm around the laser spot.

Although the best fs ablation resolution observed to date is obtained in multi-pulse exposure,¹¹ this regime requires high-numerical aperture focusing (hence very precise sample positioning) and can compromise the purity of the graphene.¹⁰ Our recent studies indicate that fs pulses with Bessel beam profiles provide significant advantages on thin-film type structures.^{13,14} In this work, we apply the Bessel beam nanostructuring method for patterning of graphene surfaces. One of the most convenient substrates for graphene is SiO₂ on Si, as it provides visibility of graphene layers even under an optical microscope. On the other hand, laser processing of graphene on this kind of substrate requires attention since the Si substrate has a significantly higher absorption and lower damage threshold, as compared to graphene. We show that, in single-pulse-ablation regime, proper adjustment of sample translation speed allows complete removal of graphene, while leaving the substrate totally intact.

In our ablation experiments, we use a chirped-pulse amplification system producing 550 fs pulses at a central wavelength of 1030 nm (Amplitude Systemes, s-pulse). The repetition rate is kept constant at 1 kHz. To improve the ablation resolution, we generate the third harmonic of the laser yielding 343 nm of wavelength. The Gaussian laser beam is converted to a Bessel beam using a 40° base angle axicon made of fused silica. The generated Bessel beam consists of a central peak of 500 nm diameter (distance between the first two zeroes), surrounded by concentric rings. We control the laser pulse energy using a waveplate and a polarizer. For all of scanning experiments discussed below, the laser polarization is set perpendicular to the direction of motion. Translation of the sample is controlled by a 3-axis piezo stage (Mad City Labs, Nano3D 200).

The commercial SLG used in the experiments (Graphene Supermarket) is first grown on copper foils and then transferred to Si/SiO₂ substrate using a poly methyl methacrylate assisted transfer method.¹⁵ The SiO₂ layer is 285 nm thick, and the surface area of the whole sample is 1 cm². Prior to

^{a)}selcuk.akturk@itu.edu.tr

ablation, Raman microscopy measurements are performed with 532 nm laser source at room temperature. We use 50 \times and 100 \times objectives, yielding 1 μm and 0.7 μm laser spot sizes, respectively. Raman spectra acquired in the range from 1200 cm^{-1} to 3000 cm^{-1} include characteristic SLG peaks (see Fig. 4). D band, which stems from defects in crystal structure, is observed at 1342 cm^{-1} while higher intensity G band from sp^2 phonon vibrations is observed at 1585 cm^{-1} . A sharp 2D peak, which also happens to be the most intense peak, is observed at 2673 cm^{-1} . The widths (FWHM) of G and 2D peaks were measured as 15 cm^{-1} and 35 cm^{-1} , respectively. The intensity ratio of I_G to I_{2D} peaks is measured as ~ 0.3 . This recipe¹⁶ verifies that our samples consist of SLG.

We scan the sample under laser irradiation using a broad range of scan speed and laser fluence values. For each parameter set, we ablate lines 100 μm long. Scanning electron microscope (SEM) and optical microscope images of typical ablation stripes are shown in Fig. 1, where the laser pulse energy is 150 nJ and scan speed is 330 $\mu\text{m}/\text{s}$. Based on the Bessel-Gauss profile calculations,¹⁷ we estimate that this energy corresponds to peak fluence around $\sim 200 \text{ mJ}/\text{cm}^2$ at the central lobe (Precise measurement of fluence is hindered by the multiple-ring nature of Bessel beams. Hence, we report our experimental findings below with reference to pulse energy). Even though the ablated stripes exhibit small-scale irregularities and sporadic discontinuities, which might result from pulse-to-pulse energy fluctuations and sample defects, it is evident that precise and sub-micron ablation of graphene is achieved with fluences near the ablation threshold.

The single-shot damage threshold fluence of graphene measured at 790 nm laser wavelength is reported to be 200 mJ/cm^2 .¹⁰ Since we work at a much shorter wavelength (343 nm), our samples experience a lower threshold fluence. Experimental results reveal that fluences as low as $\sim 150 \text{ mJ}/\text{cm}^2$ can successfully ablate graphene as explained below.

A particularly interesting result of our experiments is that, for a range of pulse energies and scan speed values (around 300 $\mu\text{m}/\text{s}$), graphene is ablated with no detectable damage on the substrate. In contrast to previous graphene on Si/SiO₂ experiments¹¹ (where a large number of pulses with a fluence well below the ablation threshold is used), we work with fluences above the single-shot ablation threshold. It is well known that SLG is mostly transparent over a broad spectral range, (e.g., more than 97% transmittivity for 300 nm $< \lambda < 1100$ nm). In the same spectral range, Si has

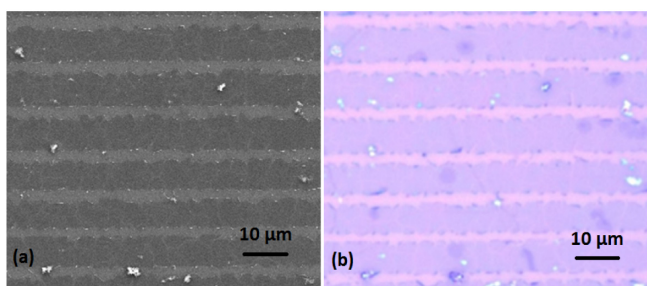


FIG. 1. (a) SEM and (b) optical microscope images of a femtosecond laser ablated stripes on SLG. Lighter regions are ablated (graphene-free) parts.

much more significant absorption. Hence, the damage threshold of Si at 343 nm is lower and is reported to be around 100 mJ/cm^2 .¹⁸ Therefore, on samples such as ours, one might expect damage on Si taking place before (or at least together with) graphene. Note that since the SiO₂ layer is more transparent than Si, we can disregard its effect for these arguments.

Our experimental results indicate that the status of the Si substrate after graphene ablation depends both on pulse energy and scan speed. It is possible to find an optimal window of pulse energy and scan speed values, over which Si receives no detectable damage. On the other hand, for an energy within this range, when the speed is reduced, the substrate starts to be damaged. Similarly, at a fixed speed, when the energy is increased, the substrate is damaged.

We attribute our observation of graphene ablation with no substrate modification to nonlinear-optical shielding by graphene. When the sample scan speed allows a few number of overlapping pulses, the incoming pulse energy is mostly absorbed by the graphene (and hence causes its removal), and the remaining energy falls below the ablation threshold of both Si and SiO₂. For translation speed of 300 $\mu\text{m}/\text{s}$, the beam moves by 300 nm between pulses. Hence, at the first Bessel peak, two pulses only partially overlap on the sample.

In order to verify this explanation, we performed the following experiments. We first ablate stripes on graphene at pulse energy-scan speed values which yields no substrate damage. Figure 2(a) shows optical microscope image of such a pattern, obtained at 120 nJ and 330 $\mu\text{m}/\text{s}$. Then, we lower the scan speed to 100 $\mu\text{m}/\text{s}$, keeping the same pulse energy (Fig. 2(b)). In this case, sufficient number of pulses overlap spatially, so that after complete graphene removal, there are still incident pulses to cause damage on Si (apparent as bright regions at the center of the ablated channels). To provide better contrast and clarity, we also include false-

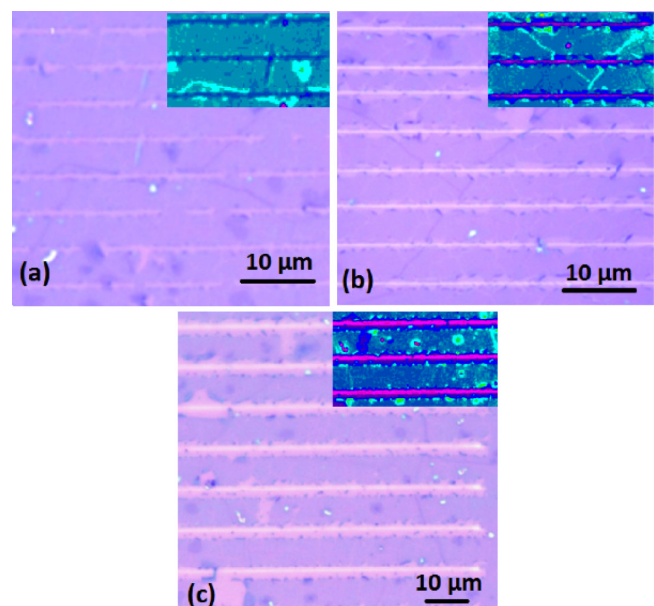


FIG. 2. Optical microscope images of produced nanostructures on monolayer graphene. Laser fluence and scan speed values are (a) 120 nJ and 330 $\mu\text{m}/\text{s}$, (b) 120 nJ and 100 $\mu\text{m}/\text{s}$, and (c) 200 nJ and 330 $\mu\text{m}/\text{s}$, respectively. Insets are false-color images, where pink regions correspond to damaged Si.

color images of ablated regions as insets. Finally, we ablate lines at $330 \mu\text{m/s}$, with 200 nJ pulse energy, which also causes Si damage (Fig. 2(c)). In this case, even though there is limited pulse overlap, the energy of the pulse is sufficiently high that even after nonlinear absorption by graphene layer, the transmitted pulse energy is still above the ablation threshold of Si. Substrate damages observed in Figs. 2(b) and 2(c) are also verified by SEM and Raman measurements. The SEM measurements taken from these regions exhibit change of contrast, whenever damage takes place. Similarly, micro-Raman measurements from damaged regions (see below for details) exhibit a drop in the Si peak at 520 cm^{-1} .

In order to determine the fabrication resolution (smallest ablation width) in our configuration, we systematically decrease the pulse energy and measure the ablation channel width. For these experiments, the scan speed is kept constant at $330 \mu\text{m/s}$. Theoretical results are obtained using 86 nJ of threshold pulse energy for the ablation of graphene.¹⁰ Both experimental and theoretical results are shown in Fig. 3, while Table I lists minimum (w_{min}), average (w_{ave}), and maximum (w_{max}) channel widths as a function of pulse energy. For energies over 100 nJ , the channel widths are above the Bessel peak diameter of 500 nm , hence, they are generated by multiple rings. The overall behavior follows the envelope of Bessel function peaks. For pulse energy below 100 nJ , only center peak causes ablation, and the smallest observable channel width in this regime is $\sim 400 \text{ nm}$. Even though one might expect much better results from extrapolation, fluences close to threshold requires extremely precise control of pulse-to-pulse stability and sample uniformity. When pulse energy is further decreased, we observe that the channels become highly discontinuous. For applications requiring better uniformity of graphene stripes, these limitations can be addressed by working with higher-quality and higher purity samples and performing the ablation in vacuum or inert gas environment.

Fabricated structures are also characterized with a Raman microscope in order to clarify graphene removal after laser irradiation. Three sets of measurements are taken on (i) ablated channels, (ii) graphene stripes between ablated lines,

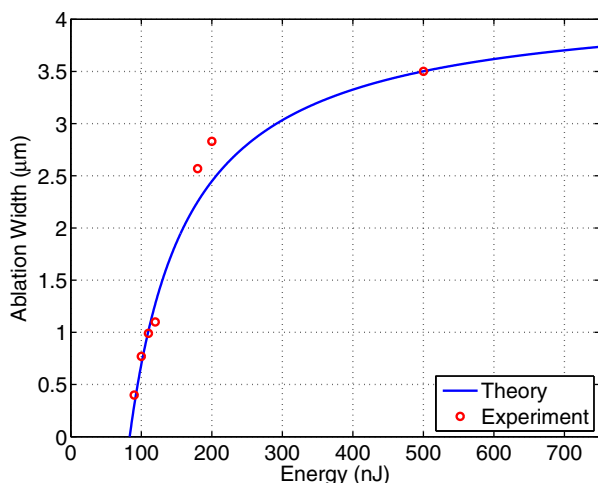


FIG. 3. Theoretical (blue solid line) and experimental (red circles) values of channel widths with respect to laser energy. In the experiments, the scan speed of sample was kept constant at $330 \mu\text{m/s}$ during the ablation process.

TABLE I. Pulse energy vs. minimum (w_{min}), average (w_{ave}), and maximum (w_{max}) channel width values.

Energy (nJ)	w_{min} (μm)	w_{ave} (μm)	w_{max} (μm)
500	3.500	3.736	3.905
200	2.830	2.990	3.240
180	2.567	2.780	2.941
120	1.100	1.280	1.424
110	0.990	1.060	1.125
100	0.770	0.830	0.885
90	0.400	0.480	0.545

and (iii) edges of the ablated regions. Fig. 4(a) compares the first two for the wavenumbers changing from 1200 cm^{-1} to 2900 cm^{-1} . The Raman spectra measured on the graphene stripe (black curve) exhibit the three characteristic peaks (D, G and 2D bands¹⁶) of a monolayer graphene, whereas spectrum taken on the ablated region indicates nearly complete removal of graphene. Fig. 4(b) compares the spectra measured on the edge of the ablated region to SLG spectra for the wavenumbers changing from 1200 cm^{-1} to 1800 cm^{-1} . There is a small increase in the D-band peak, caused by the oxidation during the ablation process on the edge.

The surfaces of the ablated samples are scanned with the aforementioned Raman microscope utilizing a $100\times$ objective. The Raman laser spot size is $0.7 \mu\text{m}$ and the laser power is adjusted carefully to prevent any thermal effect on the graphene. Fig. 5 shows optical, SEM, and Raman microscope images of a processed sample.

Last, we investigate the limits of our method in fabrication of narrow graphene stripes. We gradually decrease the distance between adjacent ablation channels, thereby generating graphene stripe arrays (Fig. 5). We observe that, in order to generate periodic stripes without complete removal, the period of structures and width of ablated lines should be kept around $1.8 \mu\text{m}$ and $0.9 \mu\text{m}$, respectively.

In conclusion, our results show that fs-pulses carry a strong potential for nano-structuring of monolayer graphene.

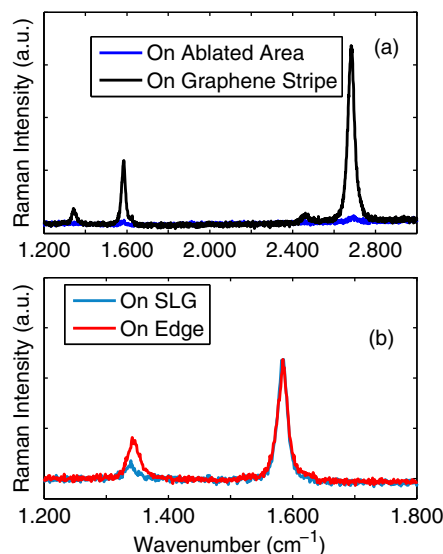


FIG. 4. Raman spectrum measurements on fabricated structures. Spectrums are obtained on three different regions on the fabricated pattern.

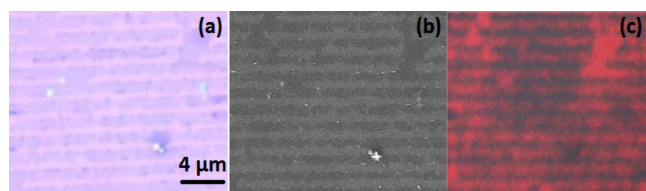


FIG. 5. (a) Optical microscope, (b) SEM, and (c) Raman 2D mapping images of same region of an ablated sample. Bright lines in (a) and (b), dark lines in (c) are the ablated parts of the SLG surface. Laser fluence and scan speed values are 120 nJ and 330 $\mu\text{m/s}$, respectively.

Maskless nanometer size resolution and periodic structures can be produced in a controllable way on SLG in ambient conditions. We optimize the laser energy and scan speed of the sample to prevent any damage on the Si/SiO₂ substrate. We show that substrate damage can be prevented by nonlinear absorption shielding of graphene. The quality of ablation process is investigated with Raman and SEM studies. Fabrication method can be extended to different substrates, which require new sets of experimental studies to prevent unwanted substrate damages.

This work was supported by Turkish Academy of Sciences (TUBA GEBIP). We also would like to thank Dr. Ozgur Birer from Koc University for SEM and Raman studies; and Dr. Oguzhan Gurlu from ITU for useful suggestions. R. Sahin also thanks TUBITAK for Ph.D. scholarship.

¹K. Novoselov, A. Geim, S. Morozov, D. Jiang, Y. Zhang, S. Dubonos, I. Grigorieva, and A. Firsov, *Science* **306**, 666–669 (2004).

²S. Stankovich, D. A. Dikin, G. H. B. Dommett, K. M. Kohlhaas, E. J. Zimney, E. A. Stach, R. D. Piner, S. T. Nguyen, and R. S. Ruoff, *Nature* **442**, 282–286 (2006).

³A. K. Geim and K. S. Novoselov, *Nature Mater.* **6**, 183–191 (2007).

⁴G. Eda, G. Fanchini, and M. Chhowalla, *Nat. Nanotechnol.* **3**, 270–274 (2008).

⁵X. Li, W. Cai, J. An, S. Kim, J. Nah, D. Yang, R. Piner, A. Velamakanni, I. Jung, E. Tutuc, S. K. Banerjee, L. Colombo, and R. S. Ruoff, *Science* **324**, 1312–1314 (2009).

⁶Y. Ye, L. Gan, L. Dai, Y. Dai, X. Guo, H. Meng, B. Yu, Z. Shi, K. Shang, and G. Qin, *Nanoscale* **3**, 1477–1481 (2011).

⁷K. S. Kim, Y. Zhao, H. Jang, S. Y. Lee, J. M. Kim, K. S. Kim, J.-H. Ahn, P. Kim, J.-Y. Choi, and B. H. Hong, *Nature* **457**, 706–710 (2009).

⁸G. Kalita, L. Qi, Y. Namba, K. Wakita, and M. Umeno, *Mater. Lett.* **65**, 1569–1572 (2011).

⁹W. Zhang, L. Li, Z. B. Wang, A. A. Pena, D. J. Whitehead, M. L. Zhong, Z. Lin, and H. W. Zhu, *Appl. Phys. A: Mater. Sci. Process.* **109**, 291–297 (2012).

¹⁰A. Roberts, D. Cormode, C. Reynolds, T. Newhouse-Illige, B. J. Leroy, and A. S. Sandhu, *Appl. Phys. Lett.* **99**, 051912 (2011).

¹¹R. J. Stoehr, R. Kolesov, K. Xia, and J. Wrachtrup, *ACS Nano* **5**, 5141–5150 (2011).

¹²J.-H. Yoo, J. B. In, J. B. Park, H. Jeon, and C. P. Grigoropoulos, *Appl. Phys. Lett.* **100**, 233124 (2012).

¹³R. Sahin, Y. Morova, E. Simsek, and S. Akturk, *Appl. Phys. Lett.* **102**, 193106 (2013).

¹⁴B. Yalizay, T. Ersoy, B. Soyulu, and S. Akturk, *Appl. Phys. Lett.* **100**, 031104 (2012).

¹⁵X. Li, Y. Zhu, W. Cai, M. Borysiak, B. Han, D. Chen, R. D. Piner, L. Colombo, and R. S. Ruoff, *Nano Lett.* **9**, 4359–4363 (2009).

¹⁶A. C. Ferrari, J. C. Meyer, V. Scardaci, C. Casiraghi, M. Lazzeri, F. Mauri, S. Piscanec, D. Jiang, K. S. Novoselov, S. Roth, and A. K. Geim, *Phys. Rev. Lett.* **97**, 187401 (2006).

¹⁷J. Arit and K. Dholakia, *Opt. Commun.* **177**, 297–301 (2000).

¹⁸J. Thorstensen and S. E. Foss, *J. Appl. Phys.* **112**, 103514 (2012).